Polymer 201 (2020) 122568

Contents lists available at ScienceDirect

Polymer

journal homepage: http://www.elsevier.com/locate/polymer

Synthesis and molecular dynamic simulation of a novel single ion conducting gel polymer electrolyte for lithium-ion batteries

Xiu Shen [a], Haiming Hua [a], Hang Li [b], Ruiyang Li [a], Texiong Hu [b], Dezhi Wu [c], Peng Zhang [b,**], Jinbao Zhao [a,b,*]

[a] State Key Lab of Physical Chemistry of Solid Surfaces, Collaborative Innovation Center of Chemistry for Energy Materials, State-Province Joint Engineering Laboratory of Power Source Technology For New Energy Vehicle, College of Chemistry and Chemical Engineering, Xiamen University, Xiamen, 361005, China
[b] School of Energy Research, College of Energy, Xiamen University, Xiamen, 361102, China
[c] School of Aerospace Engineering, Xiamen University, Xiamen, 361005, China

ARTICLE INFO

Keywords:
Gel polymer electrolyte
Single ion conductor
Molecular dynamic simulation

ABSTRACT

Single ion conductor has been realized as a new path to reduce polarization and improve electrochemical performance of the lithium ion batteries (LIBs). In this work, a novel single ion conductor gel polymer electrolyte (SIGPE) was designed via free radical polymerization, co-electrospinning and plasticizing process. The molecular structure information of the single ion polyanionic salt P(MPEGA-AMPSLi) of the SIGPE is carefully verified. The SIGPE shows high ionic conductivity of around 2.8×10^{-5} S/cm at 25 °C, high lithium ion transference number of 0.75, wide electrochemical window of 4.7 V as well as a stable cycle performance at 25 °C and 60 °C. The plasticizing mechanism of the gel polymer electrolyte has also been modeled and studied theoretically by molecular dynamics simulation. The results display a positive effect of the plasticizing in promoting the ionization of Li ions, increasing the diffusion coefficient of Li ions from 8.05×10^{-11} cm^2/s to 1.37×10^{-9} cm^2/s.

1. Introduction

Facing global problems of environmental pollution and energy crisis, seeking efficient and clean energy storage and conversion systems is of the key importance. Lithium ion batteries (LIBs) have been intensively studied as a high density energy storage source, widely applied in electric and vehicle electric field [1–4]. Commercial liquid electrolyte used in LIBs is usually a solution dissolving lithium salt into carbonate solvents to obtain high ionic conductivities, meanwhile suffering safety issues like leakage and inflame due to the low flash point of nonaqueous solvents [5,6]. Solid state electrolytes were born and become noticeable to solve this problem which could be classified into inorganic solid electrolytes (ISEs) and solid polymer electrolytes (SPEs) [7,8]. SPEs are more flexible to design the shape and package compared with the inorganic solid electrolytes [9]. However, their ionic conductivity at room temperature is too low (10^{-7}-10^{-6} S/cm) to meet the practical usage requirements [10,11]. For instance, the only commercial SPE is PEO and LiTFSI system for electric automobile named “autolib”, however, it has to be heated over 60 °C at first to start [12]. According to the state of art, SPEs could be improved by liquid plasticizing to gain acceptable ionic conductivity at room temperature and the gel polymer electrolyte (GPEs) has been proposed as a compromising method for the commercial applications [13]. GPEs were mostly based on composites of lithium salts and macromolecules such as PEO [14,15], polyvinylidene fluoride-hexafluoroproperlyene (PVDF-HFP) [16–18], polyacrylonitrile (PAN) [19,20], polymethal methacrylate (PMMA) [21,22], etc. However, they are usually dual-ion conductor, in which anions and cations migrate at the same time, the Li-ion transference number is usually around 0.3, resulting in concentration gradients and battery polarization due to the anions’ deposition and side reaction on the surface of anode [23]. Single ion conductor with high selective of ion conduction was proposed and aroused intense research concern [24].

The single ion conductor is usually composed of a polymer chain with anions anchored on the skeleton and Li ions associated with the anions, with Li ions as the only charge carrier conducted through electrolyte, eliminating the anion polarization at the interface with

* Corresponding author. State Key Lab of Physical Chemistry of Solid Surfaces, Collaborative Innovation Center of Chemistry for Energy Materials, State-Province Joint Engineering Laboratory of Power Source Technology For New Energy Vehicle, College of Chemistry and Chemical Engineering, Xiamen University, Xiamen, 361005, China.
** Corresponding author.
E-mail addresses: pengzhang@xmu.edu.cn (P. Zhang), jbzhao@xmu.edu.cn (J. Zhao).

https://doi.org/10.1016/j.polymer.2020.122568
Received 4 March 2020; Received in revised form 24 April 2020; Accepted 4 May 2020
Available online 14 May 2020

electrodes [25]. Single ion conductor has been reported showing better performance even with ten times smaller ionic conductivity than dual ion conduction electrolyte [26,27]. The membrane structure such as nanoporous structure could be significantly affected the performance of both the GPE and single ion conductor due to the enlarged surface would strengthen the interaction between the plasticizer and the polymer matrix thus promoting better ionic conduction by providing more dynamics possibility for ion transport [28,29].

2-acrylamido-2-methylpropane sulfonic acid (AMPS) is a functional monomer contains two function groups: double bond for polymerization and sulfonic acid for further lithiated into a lithium ion resource. Cross-linked PAMPS-Li has been reported as filler of PI-based gel electrolyte [30]. And polymer electrolyte with both high conductivity and mechanical strength based on AMPS monomer by pre-irradiation and grafting has been formed in our previous work [31]. And we also studied a semi-structured dense quasi solid polymer electrolyte based on cross-linked PAMPS-Li [32]. In this work, we develop a novel single ion conduction gel polymer electrolyte (SIGPE) by plasticizing the nanofiber structured P(MPEGA-AMPSLi)/PVDF-HFP (abbreviated as PLi/PVDF-HFP) composite membrane, in which AMPS-Li was further designed to copolymerize with ether based functional monomer forming polyanionic salt via free radical polymerization to increase the Li ion mobility dynamics by introducing soft PEG segment. The prepared SIGPE with the high ionic conductivity and Li ion transference number. To further investigate plasticizer effect, molecular dynamics (MD) simulation was applied to simulate the ion coordination and analyze the transport mechanism in this work.

2. Experimental details

2.1. Materials

AMPS, azodiisobutyronitrile (AIBN) were bought from Aladdin. Methoxy-polyethylene glycol acrylate (MPEGA, Mn = 480), PVDF-HFP (Mw = 455000) were bought from Sigma-Aldrich. Lithium carbonate (Li_2CO_3), N, N-dimethyl formamide (DMF), diethyl ether were bought from Sinopharm Chemical Reagent Co., Ltd. Lithium iron phosphate ($LiFePO_4$) is from Aleees of Taiwan, China. Acetylene black (AB), N-methyl-2-pyrrolidone (NMP) solvent, and poly(vinylidene fluoride) (PVDF) were bought locally. Electrolyte solvents ethylene carbonate (EC) and dimethyl carbonate (DMC) are from Zhangjiagang Guotai-Huarong New Chemical Material Corp., Ltd.

2.2. Synthesis and preparation

2.2.1. Synthesis of the single ion conducting copolymer P(MPEGA-AMPSLi)

AMPS monomer was dissolved in DMF and lithiated with stoichiometric molar ratio of Li_2CO_3 under ultrasonic dispersion. The lithiated monomer AMPS-Li solution was added into a three-neck flask and then add MPEGA monomer with a molar ratio of MPEGA: AMPS = 1 : 3. AIBN (1 mol% of AMPS) was added next as the free radical polymerization initiator. Heating and stirring the mixing solution at 70 °C for 12 h in the silicon oil bath under N_2 atmosphere created by dual exhausted pipes. After polymerization reaction, precipitating the copolymer by dropping the reaction solution into iced ether eight times the volume of the solution, obtaining white precipitate. Dissolve the white precipitate in DMF and repeat the dissolution and precipitation for at least three times for separation and purification, and dry the product within vacuum oven at 80 °C for 2 days, obtaining the single ion conductor polyanionic salt marked as P(MPEGA-AMPSLi).

2.2.2. Preparation of the SIGPE

Dissolve 0.75 g PVDF-HFP in DMF to form a 15 wt% solution. Then mix the solution with different proportions of the synthesized P(MPEGA-AMPSLi) (0.35 g, 0.5 g) to form the electrospinning solution. Higher polyanionic salt amount of 0.65 g would cause improper electrospinning condition, influencing fiber morphology. Transfer the spinning solution into the injection syringe and control the electrospinning parameters as: 15 kV, −1 kV, 300 μL/h. Collect the nonwoven membrane and dry it in vacuum oven at 80 °C for 24 h. Then the composite PLi/PVDF-HFP membrane is obtained. With the addition of 15 μL carbonate plasticizer of ethylene carbonate (EC) and dimethyl carbonate (DMC) (1:1, in volume ratio), the SIGPE is obtained.

2.3. Assemble of the batteries

The cathode is a uniform mixture of spinel-type $LiFePO_4$, acetylene black, and PVDF with a ratio of 8:1:1, coating on the aluminum foil. And the anode is lithium pallet. The cathode, the prepared SIGPE and the anode were packaged in 2016-type coin cells to test the cycling performance.

2.4. Characterizations

The field emission scanning electron microscopes (FE-SEM, Hitachi, 4800) and the matched energy dispersive spectroscopy (EDS) were applied to investigate the morphology and the elemental distribution of the PLi/PVDF-HFP membrane. The physical morphology and roughness were also examined by the three-dimensional laser scanning confocal microscope (LSCM, VK-X250K, KEYENCE Corp.). Then the molecular structure information of the polyanionic single ion conductor salt P (MPEGA-AMPS-Li) was studied carefully by Fourier transform infrared spectroscopy (FT-IR, Nicolet IS5, Thermo Fisher Scientific Inc.) with the wavenumber range of 400–4000 cm^{-1} and nuclear magnetic resonance (NMR, 400M, Bruker). The static light scatter instrument (SLS, BI-200SM, Brookhaven Instruments Corp.) was applied to measure the weight-average molecular weight of the P(MPEGA-AMPSLi). The glass transition temperature was measured on DSC 214 polyma (NETZSCH) instrument with nitrogen gas at a heating rate of 10 °C/min while the thermosgravimetry (TG) curve of the SIGPE membrane was detected by STA 449 (NETZSCH) to investigate the decomposition temperature.

The ionic conductivity (σ) was investigated and calculated by electrochemical impedance spectroscopy (EIS) method with following the equation (1):

$$\sigma = d / (R_b \times S) \quad (1)$$

where d represents the thickness of the SIGPE membrane, R_b stands for the bulk resistance of the SIGPE obtained by alternating current (AC) impedance, S refers to the work electrode area of the stainless steel (SS) sheet. The AC impedance was measured by the Solartron (SI-1260) electrochemical workstation with a frequency range of 10^{-1}–10^5 Hz. The electrochemical window was measured by linear sweep voltammograms (LSV) of Li/SIGPE/SS cell at a scan rate of 0.5 mV/s in order to study the chemical stability of the SIGPE.

The lithium ion transference number (LTN) was tested by chronoamperometry methods using the Autolab (Sino-Metrohm Technology Ltd) electrochemical work station. The LTN was obtained by the combination of the direct current (DC) polarization and AC impedance measured on the symmetric Li | SIGPE | Li cell, following equation (2):

$$t_{Li}^{+} = I_s (\Delta V - I_0 R_0) / I_0 (\Delta V - I_s R_s) \quad (2)$$

in which ΔV is the applied polarization voltage of 10 mV; I_0 and I_s are the polarization current at the beginning and after the polarization, respectively; R_0, R_s stand for the initial and final impedance of the cell of the polarization process, respectively.

The charge/discharge performance of the assembled CR2016 Li/$LiFePO_4$ coin cells were operated at the voltage range of 2.5–3.7 V on the NEWARE battery testing system (BTS-610, Neware Technology Co., Ltd.). Both 25 °C and 60 °C was set to inspect the electrical performance of the cells.

2.5. Simulation information

The molecular dynamics simulation and result analysis were performed using GROMACS 2018 [33] software. The Visualization of structures were performed by VMD software [34] and CYLview software [35].The structure of the two repeat segment unit (MPEGA and AMPS-Li) of the single ion conductor and plasticizer molecules were optimized at B3LYP-D3 [36,37]/def2-SVP [38] level with Gaussian 09 Package [39], and the partial charges on atoms were obtained using restrained electrostatic potential (RESP) method which calculated with Multiwfn software [40] at B3LYP-D3/6-311+G(d,p) [41,42] level. The electrostatic surface potential (ESP) was also calculated by Multiwfn at the same level. Force field parameters for all molecules were gotten from the general AMBER force field (GAFF) [43] using Antechamber code [44] and Acpype code [45]. The local coordination structures taken from MD Simulation were further optimized at B3LYP-D3/def2-SVP level with Gaussian 09.

A polymer chain model contains 5 AMPSLi units and 10 MPEGA units. The two structural units are arranged alternately by ABB sequence. The plasticizer-free system simulation boxes contained 100 Li cations, and 20 polymer chains. The plasticizer system simulation boxes contained 40 Li cations, and 8 polymer chains 483 EC molecules and 326 DMC molecules. All systems were generated by Packmol software [46].

All the simulation boxes were firstly submitted to energy minimization using the steepest-descent method. The equilibrium runs were carried out under the NPT ensemble at 1 bar. In order to gain an equilibrium system, an annealing method was used. The plasticizer-free system ran at 598.15 K for 50 ns, and then cooled to 298.15 K within 50 ns, then ran at 298.15 K for 100 ns. Plasticizer system ran at 398.15 K for 50 ns and then cooled to 298.15 K within 50 ns, then ran at 298.15 K for 100 ns. The production runs were 40 ns long at 298.15 K. A time step of 2 fs and a Verlet algorithm were used. An Ewald summation routine was used for long-range forces (rcut = 10 Å), and data were collected every 2 ps.

3. Results and discussion

The synthetic route of the PLi/PVDF-HFP membrane and the SIGPE are shown in Fig. 1. Firstly, the single ion conductor polyaionic salt P (MPEGA-AMPSLi) as the lithium source for the electrolyte with -SO_3Li anchored on the polymer skeleton was synthesized by free radical polymerization with AIBN as radical initiator. Secondly, the P(MPEGA-AMPSLi) was co-electrospinned with PVDF-HFP to form the nanofiber with nanoporous structured PLi/PVDF-HFP. With the nanoporous structure, the SIGPE membrane could rapidly adsorb plasticizer, swell and form lots of amorphous region [28] for better segment motion and ion conduction within the SIGPE system, leading to high ionic conductivity.

It is observed from the SEM morphology that the composite PLi/PVDF-HFP membrane shows uniform nanofiber structure (Fig. 2a). By statistics and analyzing of the diameter distribution with Image pro plus (Ipp) software, the diameter is found fitting well with normal distribution (Fig. 2b), mainly located in 700–800 nm interval. And this is tunable by changing electrospinning conditions. As seen from the surface SEM image and the corresponding element mapping results, F, O, S atoms are evenly distributed through the whole membrane (Fig. 2c-2f) and this suggests a uniform distribution of single ion conductor polyanionic salt P(MPEGA-AMPSLi) and PVDF-HFP in the electrospinning nanofiber. The uniform distribution of salt is greatly beneficial for the uniform current density, which may result in uniform lithium deposition [28]. Further LSCM image of the PLi/PVDF-HFP (Fig. 2g) shows the flat membrane morphology, consistent with the SEM results, good for the close contact with the electrodes.

FT-IR was applied to confirm the chemical structure of the P (MPEGA-AMPSLi) single ion conducting polymer salt and the PLi/PVDF-HFP composite membrane. The FT-IR spectra of AMPS monomer, P(MPEGA-AMPSLi), bare PVDF-HFP and PLi/PVDF-HFP membrane were tested (Fig. 3). Compared with AMPS monomer, P(MPEGA-AMPSLi) after polymerization, the stretching peak of C=C at 1610 cm^{-1} disappeared, indicating the success of the polymerization and no AMPS monomer left. And C=O stretching vibration peak from MPEGA monomer at 1730 cm^{-1} appeared in the copolymer after polymerization, at the same time, the asymmetric stretching of O=S=O bond of AMPS monomer changed from 1240 cm^{-1} to the 1230 cm^{-1} after polymerization. Besides, the C-S bond shows a blue shift of the adsorption peak from 628 cm^{-1} to 630 cm^{-1} due to the exchange of proton to Li-ion on AMPS [32,47]. This typical infrared absorption peaks of C-S of P (MPEGA-AMPSLi) was also shown in the PLi/PVDF-HFP membrane, indicating the successful composite of the single ion conductor polyanionic salt P(MPEGA-AMPSLi) and PVDF-HFP in the PLi/PVDF-HFP.

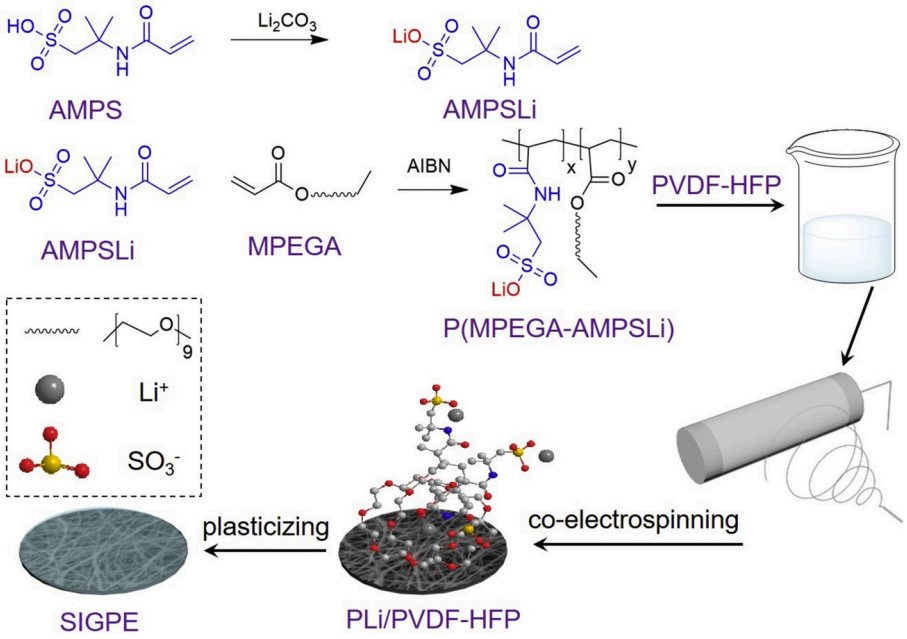

Fig. 1. Synthesis route diagram of the PLi/PVDF-HFP membrane and the SIGPE.

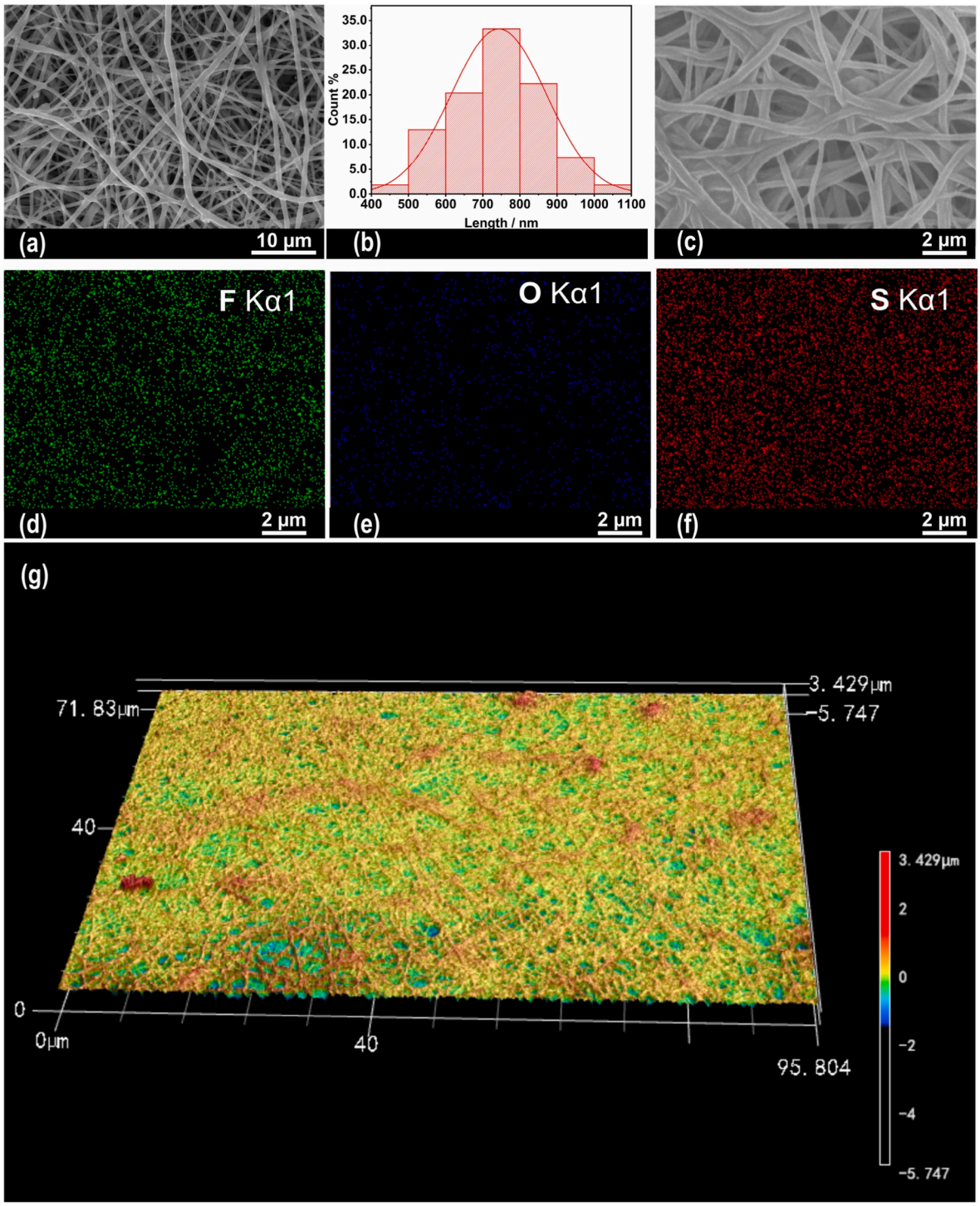

Fig. 2. (a) SEM morphology and (b) the nanofiber diameter distribution of the PLi/PVDF-HFP membrane; (c-f) Surface SEM image of PLi/PVDF-HFP and the corresponding element mapping of F, O, S atom, respectively; (g) LSCM image of the PLi/PVDF-HFP membrane.

^{1}H NMR was also applied to further investigate the molecular structure of the copolymer. ^{1}H NMR (DMSO-d_6) spectra of AMPS, MPEGA monomer and their copolymer P(MPEGA-AMPSLi) were shown in Fig. 4. The monomer results were agree well with the AMPS [31] and MPEGA [26,48] monomer. Peak 'S1', 'S2' at δ 3.34 ppm and 2.5 ppm is due to the water and DMSO-d_6 solvents. S1 for AMPS shifts to low field due to it is easy to adsorb water [31]. The resonances at ^{1}H NMR (400 MHz, DMSO) δ 8.34 (s, 1H), 6.02 (qd, J = 17.1, 6.1 Hz, 2H), 5.51 (dd, J = 9.9, 2.4 Hz, 1H), 2.82 (s, 2H), 1.43 (s, 6H), representing the H atoms of peak 'c', 'a', 'b', 'e' and 'd' on the AMPS monomer, respectively. And the integration area ratio of these peak is 1:2:1:2:6 (Fig. S1), corresponding to the hydrogen numbers of AMPS. And for the copolymer, peaks of a, b, g, k disappear, indicating the reaction of the C=C bond, suggesting the success of polymerization, consistent with IR results. Besides, the copolymer contains peak 2 (peak d, -CH_3), peak 3 (peak c, -NH-) of AMPS which becomes broader due to the polymerization, and peak 1 (corresponding to peak f, typical -CH_2CH_2O bond of MPEGA). Above results shows the success of the polymerization. By integration of the peak area [49] coupled with hydrogen number according to -CH_2CH_2O and -NH-, the molar ratio of MPEGA unit and AMPS-Li unit was obtained

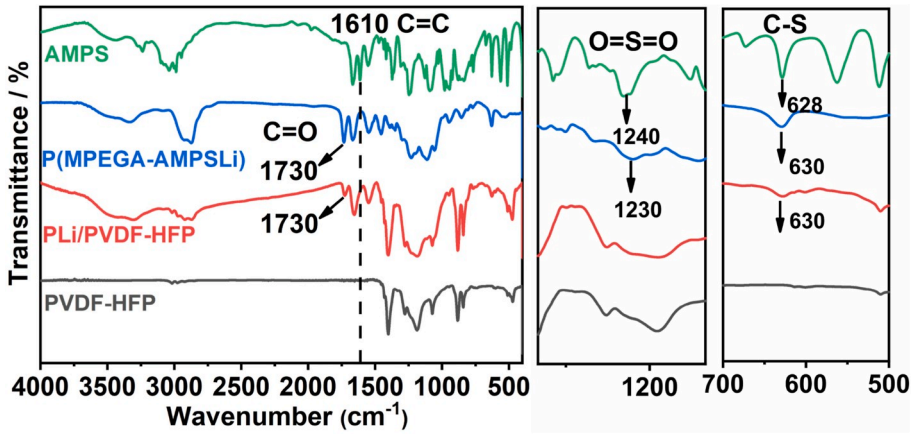

Fig. 3. The FT-IR spectra of AMPS, P(MPEGA-AMPSLi), composite PLi/PVDF-HFP membrane and pure PVDF-HFP membrane, in color of green, blue, red and black, respectively. (For interpretation of the references to color in this figure legend, the reader is referred to the Web version of this article.)

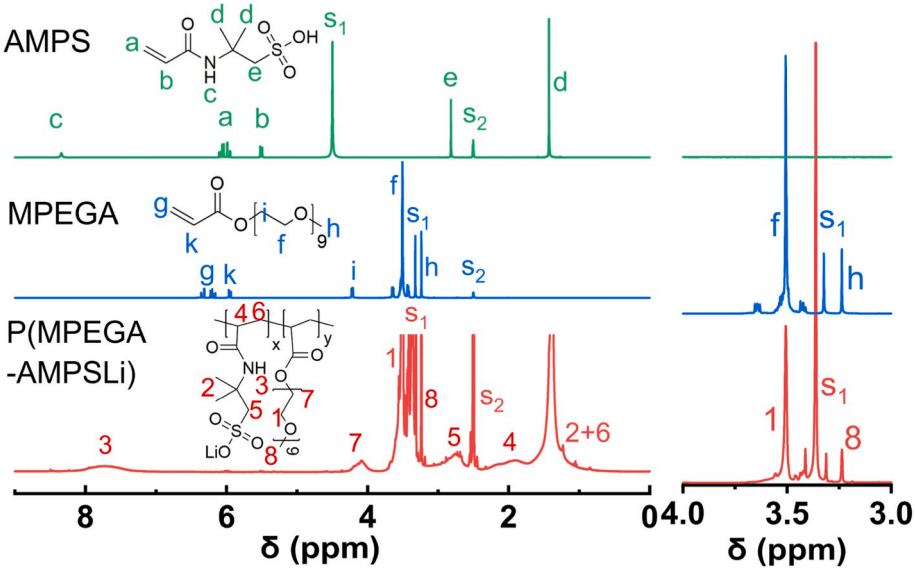

Fig. 4. ^{1}H NMR of AMPS, MPEGA monomer and P(MPEGA-AMPSLi) in DMSO-d_6.

as y: x = 2.08.

The weight-average molecular weight of the copolymer P(MPEGA-AMPSLi) was measured by a standard SLS method. The scatter intensity of different concentration and different incident angle was all measured and fitted (Fig. S3). And the zimm plot shows that the single ion conducting polyanionic salt P(MPEGA-AMPSLi) shows high weight-average molecular weight (Mw = 8.0×10^6 g/mol). Further detecting of the glass transition temperature show a value 45 °C of the P(MPEGA-AMPSLi) single ion conductor salt, determined by DSC curves from −40–100 °C in argon atmosphere at a heating rate of 10 °C/min (Fig. S2). Besides, a high decomposition temperature of 288 °C in argon atmosphere for the PLi/PVDF-HFP membrane was obtained through TG measurement (Fig. 5). The decomposition started temperatures at 288 °C, 303 °C and 410 °C are attributed to carbonlization of PEG segment [50], loss of -SO_3^- [51] of the P(MPEGA-AMPSLi) and decomposition of PVDF-HFP, which shows the most biggest decomposition rate at 442 °C. The TG results shows a stable thermal stability of the PLi/PVDF-HFP membrane up to 288 °C.

The lithium ion transference number was calculated as $t_{Li}^+ = 0.75$, shown in Fig. 6a, higher than usual gel polymer electrolyte (0.2–0.4), revealing the single ion property. The Li^+ dominating conduction is good for decreasing polarization by immobilizing anions on the backbone of the polymer chain. There maybe two main reasons for the t_{Li}^+ not being unity [52]: 1) the short-range motion of anions among the space of polymer segments; 2) the plasticizing effect on the slightly bulk motion of macromolecular skeleton. Fig. 6b shows the electrochemical window of the SIGPE, which is stable up to 4.75 V (vs. Li/Li^+), indicating

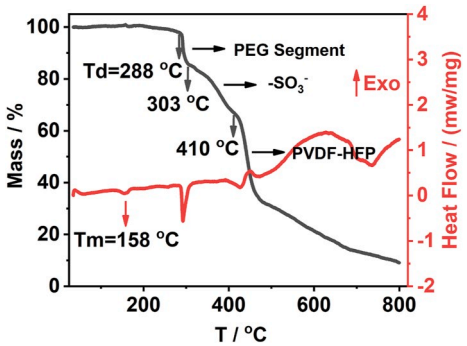

Fig. 5. TG and DSC curves of PLi/PVDF-HFP membrane measured from 35–800 °C in argon atmosphere at a heating rate of 5 °C/min.

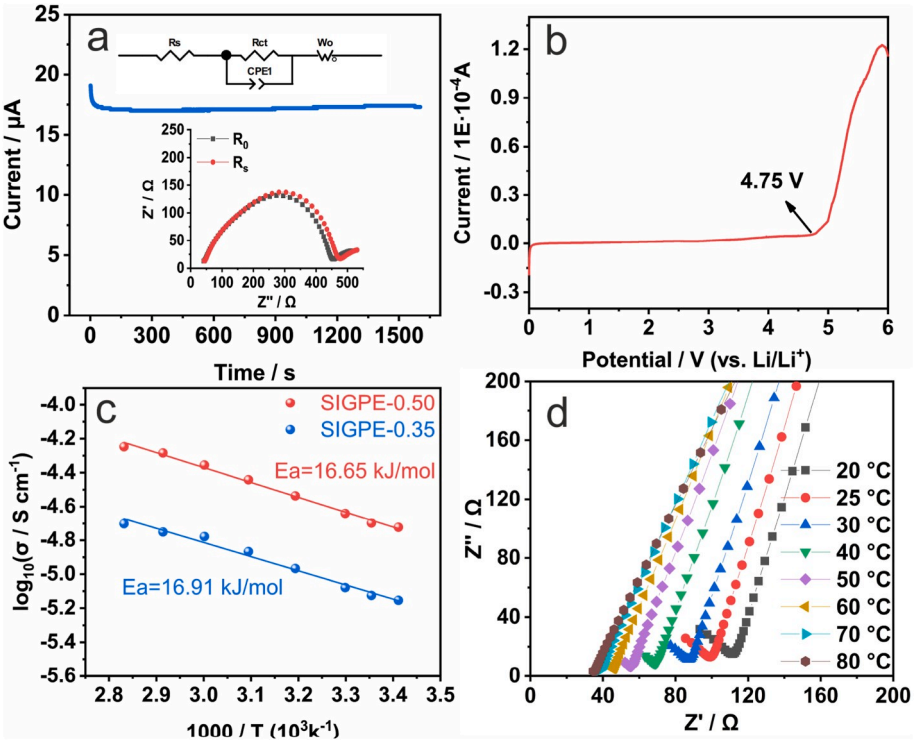

Fig. 6. (a) Lithium ion transference number plot of SIGPE. (b) The electrochemical window of the SIGPE. (c) Ionic conductivity change with temperature ranging from 20 °C–80 °C of the SIGPE with different ratio. (d) AC impedance of block cells of SS|SIGPE-0.5|SS at different temperature.

a broad oxidation resistance electrochemical window. Fig. 6c shows the dependence of ionic conductivity on temperature ranging from 20 °C to 80 °C of two different ratio of electrospinning SIGPE membrane. With the higher amount of polyanioic salt P(MPEGA-AMPSLi) (fom 0.35 g to 0.5 g), the higher ionic conductivity would be acquired. Both the results of the two ratio follows Arrhenius Equation (Eq. (3)):

$$\sigma = \sigma_0 \exp(-Ea / RT) \quad (3)$$

in which σ_0 stand for pre-exponential factor, respectively. *Ea* is on behalf of the activation energy of the ion transport; *R* represents 8.314 J/mol/K, the molar gas constant. The results indicate that SIGPE-0.5 has the lower activation energy of 16.65 kJ/mol than that of SIGPE-0.35 of 16.91 kJ/mol, revealing a lower energy barrier of ion motion. Fig. 6d shows the AC impedance of the block cell with SIGPE-0.5 electrolyte at different temperature. The calculated ionic conductivities of SIGPE-0.5 was around 2.8×10^{-5} S/cm at 25 °C, indicating the stability ionic transport performance of the SIGPE. The ionic conductivity value is one of the highest value among single ion conductor gel electrolytes [25,53,54] in recent years and also higher than PAMPS-Li based single ion conductor gel polymer electrolyte (Fig. S4) due to the lower activation energy.

Electrochemical performance of the SIGPE-assembled battery has been studied at different temperature and the schematic diagram of the assembled cell is shown in Fig. 7a. Fig. 7b shows the charge-discharge cycle and rate performance of SIGPE coin cells at 25 °C. The first discharge capacity is up to 146.2 mA h/g with a coulombic efficiency of 96.5%. 94.0% of the discharge capacity maintained after 100 cycles charge/discharge process, showing a stable cycling performance. Besides, the capacity-voltage curves are also examined at the 1st, 20th, 50th cycle (Fig. 7c). The charge-discharge plateaus show no distinct widen, owing to the advantage of the single ion conductor, which suppressing the anions' polarization by immobilize them on the polymer chain. Fig. 7d shows a good rate performance of the SIGPE assembled battery, and when the rate came back to the small level of 0.2 C, the discharge capacity could also went back to initial value, suggesting a good rate performance. High temperature cycle performance was further studied with the SIGPE. Cells with SIGPE show their superiority cycling at 60 °C at 0.2 C even 0.5 C, during which process the coulombic efficiency is close to 100%. At 0.2 C (Fig. 7e) and 0.5 C (Fig. 7f), the initial discharge capacity could reach 164.6 and 138.9 mA h/g. After 100 cycle, the capacity could maintain 88.7% and 86.4% at 0.2 C and 0.5 C, respectively. Compared with Li/$LiFePO_4$ cells at 60 °C with liquid electrolyte (1M $LiPF_6$ in EC: DMC = 1: 1, in volume) , which shows obvious overcharge, with low columbic efficiency less than 80% (Fig. S5), the SIGPE battery shows stable cycle performance at high temperature. This is because the $LiPF_6$ is easy to decompose under high temperature in battery [28,55] and the decomposition product of hydrogen fluoride (HF) will cause the dissolution of the $LiFePO_4$ cathode [56]. By cycle performance contrast, the SIGPE containing polyanionic salt of P(MPEGA-AMPSLi) shows stable chemical window and cycle stability.

According to the reference, single ion conductor could do good for the deposition of the lithium for no anions' depletion [10] and GPE is considered as an effective way for building safer lithium metal battery [57]. So lithium symmetric experiment with SIGPE and commercial liquid electrolyte system (PP-LE) was carried out (Fig. S6). The results show that the SIGPE and the commercial liquid electrolyte show similar polarization voltage, while the liquid electrolyte became larger slowly. The larger polarization after long cycle for the liquid electrolyte is mainly due to the anions' deposition and side reaction on the electrode, which will be bad for the cycle performance. And the stable deposition-stripping of SIGPE shows the superiority of the single ion conductor on inhibiting the anion polarization.

In order to explain the plasticizing mechanism of the SIGPE system and make clear the Li-ion coordinate information, molecular dynamics simulation has been applied and analyzed. The radial distribution function (RDF) of Li^+ and the coordination number integrated from RDF before and after plasticizing was shown in Fig. 8a and 8b. Before plasticizing, the coordination number of Li^+ with O atoms of sulfonate reaches 2.1. The high coordination number indicates a tightly binding of

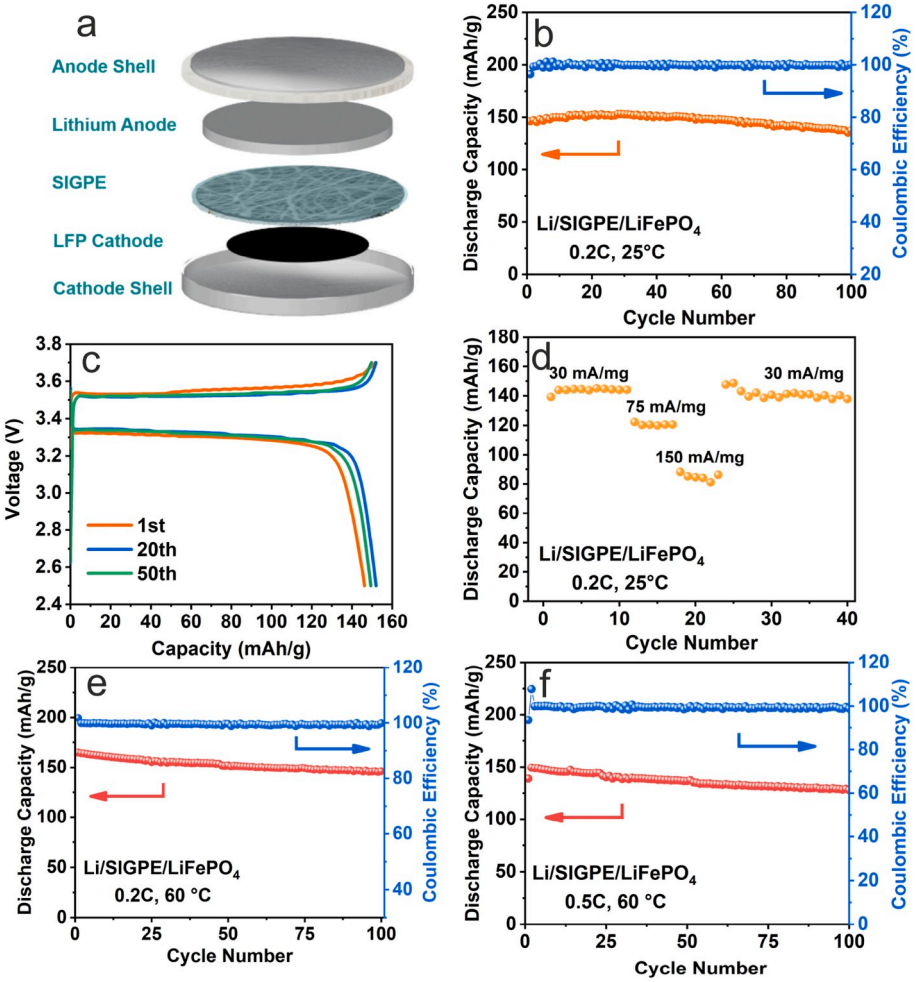

Fig. 7. (a) Schematic diagram of the SIGPE assembled cell; Cycle performance (b), voltage-capacity plots of the 1st, 20th and 50th cycle (c) and rate performance (d) of the SIGPE assembled Li/$LiFePO_4$ battery at 25 °C; Cycle performance of SIGPE assembled Li/$LiFePO_4$ coin cell with at high temperature of 60 °C with charge-discharge rate of (e) 0.2 C, (f) 0.5 C.

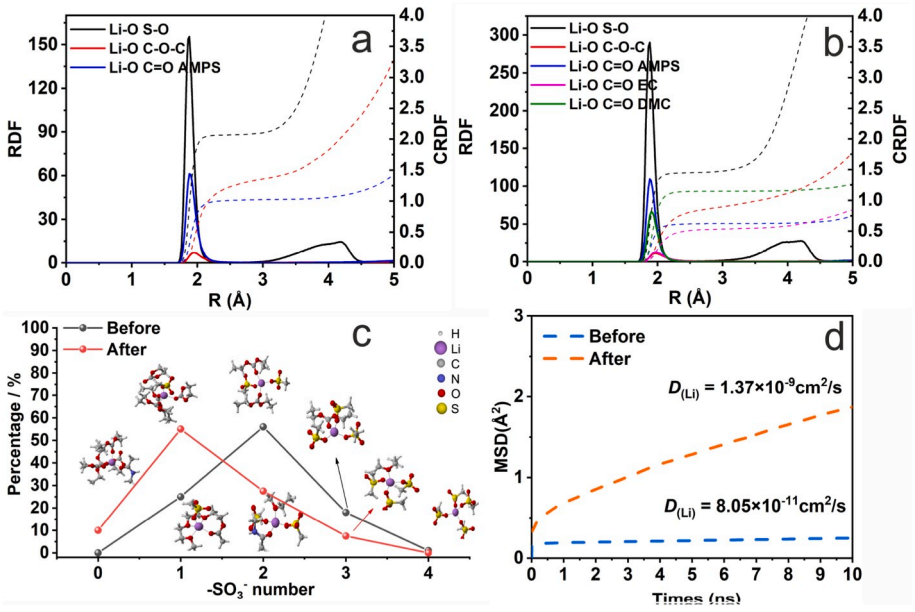

Fig. 8. Molecular dynamics simulation at 298.15 K. The radial distribution function (solid line) of Li^+ and coordination number (dashed line) of different Li-O before (a) and after plasticizing (b); (c) The ratio of Li^+ coordinated with different amount of $-SO_3^-$; (e) MSD curves before and after plasticizing. Inside figures are the corresponding snap photos where only Li (blue) and S (orange) atoms are shown. (For interpretation of the references to color in this figure legend, the reader is referred to the Web version of this article.)

sulfonate and Li^+, which cause few free Li^+ in system. The reason why the sulfonate shows a strong binding ability to Li^+ is that the maximum electrostatic surface potential (ESP) of sulfonate (−135 kJ/mol) is much more negative than that of traditional lithium salts such as PF_6^- (−119 kJ/mol) and ClO_4^- (−125 kJ/mol), which shows stronger coulomb attraction to lithium ions. After adding EC/DMC plasticizer, the coordination number of lithium to sulfonate oxygen reduced to 1.4, and that to carbonyl oxygen atoms of EC/DMC increased to 1.6, which shows Li cations are more easily to ionize. The ratio of Li cation with different coordination number to sulfonate (Fig. 8c) reflect the promoting of ionization clearly. After adding plasticizer, the rate of high coordination number (n = 2, 3, 4) decreases while the rate of low coordination number (n = 0, 1) increases obviously. Specially, the rate of 'free' (n = 0) Li cations increases from none to 10%. The promoting of ionization can significantly improve the conductivity. Why the addition of plasticizer can enhance the ionization of Li cations? On the one hand, these highly polar molecules act on dielectric polarization among anions and cations, thereby weakening the coulomb attraction between SO_3^- and Li^+. On the other hand, the carbonyl oxygen atom has a strong coordination ability, thereby participating in the coordination with Li-ions. The MSD function (Fig. 8d) indicates that the diffusion coefficient of Li^+ (D_{Li}) is greatly increased from 8.05×10^{-11} cm^2/s to 1.37×10^{-9} cm^2/s after the addition of the plasticizer, qualitatively descripting the result that the Li cation mobility is greatly improved.

4. Conclusion

In this work, a novel single ion conduction gel polymer electrolyte (SIGPE) with nanofiber structure is prepared by plasticizing of the co-electrospinning membrane PLi/PVDF-HFP, in which the novel single ion conductor polyanionic salt of P(MPEGA-AMPSLi) is synthesized by free radical polymerization. The molecular structure of the single ion polyanionic salt P(MPEGA-AMPSLi) has been verified by FT-IR and ^1H NMR. Thus SIGPE shows high ionic conductivity of 2.8×10^{-5} S/cm at 25 °C. Besides, a stable cycle performance is obtained at room and high temperature of 60 °C. By molecular dynamics simulation, the plasticizing mechanism model is built and has been studied theoretically. The coordination number with $-SO_3^-$ is decreased and the bonding is weakened after plasticizing, promoting Li^+ transfer. Besides, diffusion coefficient of Li^+ is greatly increased from 8.05×10^{-11} cm^2/s to 1.37×10^{-9} cm^2/s, indicating the addition of plasticizer will promote the ionization of the Li^+, which is due to their high dielectric constant and coordination ability, thus improving the ionic conductivity.

Declaration of competing interest

The authors declare that they have no known competing financial interests or personal relationships that could have appeared to influence the work reported in this paper.

CRediT authorship contribution statement

Xiu Shen: Conceptualization, Methodology, Writing - original draft. **Haiming Hua:** Software, Data curation, Writing - original draft. **Hang Li:** Data curation. **Ruiyang Li:** Visualization. **Texiong Hu:** Investigation. **Dezhi Wu:** Validation. **Peng Zhang:** Supervision, Writing - review & editing. **Jinbao Zhao:** Project administration, Funding acquisition.

Acknowledgement

Xiu Shen and Haiming Hua contribute equally to the article. The authors gratefully acknowledge financial support from the National Natural Science Foundation of China (Grant Numbers 21503180, 21621091, 21875195, 21875198), the Fundamental Research Funds for the Central Universities (Grant Number 20720170037) and the National Key Research and Development Program of China (Grant Number 2017YFB0102000). The authors wish to thank Prof. Weitai Wu of Xiamen University for providing molecular weight measurement.

Appendix A. Supplementary data

Supplementary data to this article can be found online at https://doi.org/10.1016/j.polymer.2020.122568.

References

[1] J.W. Choi, D. Aurbach, Promise and reality of post-lithium-ion batteries with high energy densities, Nat. Rev. Mater. 1 (4) (2016).
[2] V. Etacheri, R. Marom, R. Elazari, G. Salitra, D. Aurbach, Challenges in the development of advanced Li-ion batteries: a review, Energy Environ. Sci. 4 (9) (2011) 3243.
[3] Y. Sun, N. Liu, Y. Cui, Promises and challenges of nanomaterials for lithium-based rechargeable batteries, Nat. Energy (2016) 16071.
[4] J.M. Tarascon, M. Armand, Issues and challenges facing rechargeable lithium batteries, Nature 414 (6861) (2001) 359–367.
[5] O.W. Sheng, C.B. Jin, J.M. Luo, H.D. Yuan, H. Huang, Y.P. Gan, J. Zhang, Y. Xia, C. Liang, W.K. Zhang, X.Y. Tao, $Mg_2B_2O_5$ nanowire enabled multifunctional solid-state electrolytes with high ionic conductivity, excellent mechanical properties, and flame-retardant performance, Nano Lett. 18 (5) (2018) 3104–3112.
[6] X. Zhang, T. Liu, S.F. Zhang, X. Huang, B.Q. Xu, Y.H. Lin, B. Xu, L.L. Li, C.W. Nan, Y. Shen, Synergistic coupling between $Li_{6.75}La_3Zr_{1.75}Ta_{0.25}O_{12}$ and poly(vinylidene fluoride) induces high ionic conductivity, mechanical strength, and thermal stability of solid composite electrolytes, J. Am. Chem. Soc. 139 (39) (2017) 13779–13785.
[7] J. Wan, J. Xie, X. Kong, Z. Liu, K. Liu, F. Shi, A. Pei, H. Chen, W. Chen, J. Chen, X. Zhang, L. Zong, J. Wang, L.Q. Chen, J. Qin, Y. Cui, Ultrathin, flexible, solid polymer composite electrolyte enabled with aligned nanoporous host for lithium batteries, Nat. Nanotechnol. 14 (7) (2019) 705–711.
[8] S.A. Pervez, M.A. Cambaz, V. Thangadurai, M. Fichtner, Interface in solid-state lithium battery: challenges, progress, and outlook, ACS Appl. Mater. Interfaces 11 (25) (2019) 22029–22050.
[9] H.W. Zhai, P.Y. Xu, M.Q. Ning, Q. Cheng, J. Mandal, Y. Yang, A flexible solid composite electrolyte with vertically aligned and connected ion-conducting nanoparticles for lithium batteries, Nano Lett. 17 (5) (2017) 3182–3187.
[10] K. Deng, J. Qin, S. Wang, S. Ren, D. Han, M. Xiao, Y. Meng, Effective suppression of lithium dendrite growth using a flexible single-ion conducting polymer electrolyte, Small (2018), e1801420.
[11] Q.W. Pan, D.M. Smith, H. Qi, S.J. Wang, C.Y. Li, Hybrid electrolytes with controlled network structures for lithium metal batteries, Adv. Mater. 27 (39) (2015) 5995–6001.
[12] Q. Ma, H. Zhang, C. Zhou, L. Zheng, P. Cheng, J. Nie, W. Feng, Y.S. Hu, H. Li, X. Huang, L. Chen, M. Armand, Z. Zhou, Single lithium-ion conducting polymer electrolytes based on a super-delocalized polyanion, Angew. Chem. Int. Ed. 55 (7) (2016) 2521–2525.
[13] Y.B. Sun, R. Rohan, W.W. Cai, X.F. Wan, K. Pareek, A. Lin, Z. Yunfeng, H.S. Cheng, A polyamide single-ion electrolyte membrane for application in lithium-ion batteries, Energy Technol. 2 (8) (2014) 698–704.
[14] F. Croce, G.B. Appetecchi, L. Persi, B. Scrosati, Nanocomposite polymer electrolytes for lithium batteries, Nature 394 (6692) (1998) 456–458.
[15] C.H. Wang, Y.F. Yang, X.J. Liu, H. Zhong, H. Xu, Z.B. Xu, H.X. Shao, F. Ding, Suppression of lithium dendrite formation by using LAGP-PEO (LiTFSI) composite solid electrolyte and lithium metal anode modified by PEO (LiTFSI) in all-solid-state lithium batteries, ACS Appl. Mater. Interfaces 9 (15) (2017) 13694–13702.
[16] X. Zuo, X.X. Ma, J.H. Wu, X. Deng, X. Xiao, J.S. Liu, J.M. Nan, Self-supporting ethyl cellulose/poly(vinylidene fluoride) blended gel polymer electrolyte for 5 V high-voltage lithium-ion batteries, Electrochim. Acta 271 (2018) 582–590.
[17] G. Chen, F. Zhang, Z. Zhou, J. Li, Y. Tang, A flexible dual-ion battery based on PVDF-HFP-modified gel polymer electrolyte with excellent cycling performance and superior rate capability, Adv. Energy Mater. 8 (25) (2018) 1801219.
[18] J. Jie, Y. Liu, L. Cong, B. Zhang, W. Lu, X. Zhang, J. Liu, H. Xie, L. Sun, High-performance PVDF-HFP based gel polymer electrolyte with a safe solvent in Li metal polymer battery, J. Energy. Chem. 49 (2020) 80–88.
[19] C.F. He, J.Q. Liu, J. Li, F.F. Zhu, H.J. Zhao, Blending based polyacrylonitrile/poly (vinyl alcohol) membrane for rechargeable lithium ion batteries, J. Membr. Sci. 560 (2018) 30–37.
[20] X.J. Ma, P. Kolla, R.D. Yang, Z. Wang, Y. Zhao, A.L. Smirnova, H. Fong, Electrospun polyacrylonitrile nanofibrous membranes with varied fiber diameters and different membrane porosities as lithium-ion battery separators, Electrochim. Acta 236 (2017) 417–423.
[21] Y. Li, K.W. Wong, Q.Q. Dou, K.M. Ng, A single-ion conducting and shear-thinning polymer electrolyte based on ionic liquid-decorated PMMA nanoparticles for lithium-metal batteries, J. Mater. Chem. 4 (47) (2016) 18543–18550.
[22] J.L. Shi, L.F. Fang, H. Li, H. Zhang, B.K. Zhu, L.P. Zhu, Improved thermal and electrochemical performances of PMMA modified PE separator skeleton prepared via dopamine-initiated ATRP for lithium ion batteries, J. Membr. Sci. 437 (2013) 160–168.
[23] Q. Ma, H. Zhang, C.W. Zhou, L.P. Zheng, P.F. Cheng, J. Nie, W.F. Feng, Y.S. Hu, H. Li, X.J. Huang, L.Q. Chen, M. Armand, Z.B. Zhou, Single lithium-ion conducting

polymer electrolytes based on a super-delocalized polyanion, Angew. Chem. Int. Ed. 55 (7) (2016) 2521–2525.
[24] H. Zhang, C. Li, M. Piszcz, E. Coya, T. Rojo, L.M. Rodriguez-Martinez, M. Armand, Z. Zhou, Single lithium-ion conducting solid polymer electrolytes: advances and perspectives, Chem. Soc. Rev. 46 (3) (2017) 797–815.
[25] S.W. Liang, Q. Chen, U.H. Choi, J. Bartels, N.Q. Bao, J. Runt, R.H. Colby, Plasticizing Li single-ion conductors with low-volatility siloxane copolymers and oligomers containing ethylene oxide and cyclic carbonates, J. Mater. Chem. 3 (42) (2015) 21269–21276.
[26] S.W. Feng, D.Y. Shi, F. Liu, L.P. Zheng, J. Nie, W.F. Feng, X.J. Huang, M. Armand, Z.B. Zhou, Single lithium-ion conducting polymer electrolytes based on poly[(4-styrenesulfonyl)(trifluoromethanesulfonyl)imide] anions, Electrochim. Acta 93 (2013) 254–263.
[27] Z.Q. Jin, K. Xie, X.B. Hong, Synthesis and electrochemical properties of a perfluorinated ionomer with lithium sulfonyl dicyanomethide functional groups, J. Mater. Chem. 1 (2) (2013) 342–347.
[28] C. Li, B. Qin, Y. Zhang, A. Varzi, S. Passerini, J. Wang, J. Dong, D. Zeng, Z. Liu, H. Cheng, Single-ion conducting electrolyte based on electrospun nanofibers for high-performance lithium batteries, Adv. Energy Mater. (2019) 1803422.
[29] R. Rohan, K. Pareek, Z.X. Chen, W.W. Cai, Y.F. Zhang, G.D. Xu, Z.Q. Gao, H. S. Cheng, A high performance polysiloxane-based single ion conducting polymeric electrolyte membrane for application in lithium ion batteries, J. Mater. Chem. 3 (40) (2015) 20267–20276.
[30] H. Zhang, Y. Zhang, Z.K. Yao, A.E. John, Y. Li, W.S. Li, B.K. Zhu, Novel configuration of polyimide matrix-enhanced cross-linked gel separator for high performance lithium ion batteries, Electrochim. Acta 204 (2016) 176–182.
[31] Y. Ding, X. Shen, J. Zeng, X. Wang, L.Q. Peng, P. Zhang, J.B. Zhao, Pre-irradiation grafted single lithium-ion conducting polymer electrolyte based on poly(vinylidene fluoride), Solid State Ionics 323 (2018) 16–24.
[32] X. Shen, L.Q. Peng, R.Y. Li, H. Li, X. Wang, B.Y. Huang, D.Z. Wu, P. Zhang, J. B. Zhao, Semi-IPN structured single-ion conduction polymer electrolyte for lithium ion batteries, ChemElectroChem 6 (17) (2019) 4483–4490.
[33] M.J. Abraham, T. Murtola, R. Schulz, S. Páll, J.C. Smith, B. Hess, E. Lindahl, GROMACS: high performance molecular simulations through multi-level parallelism from laptops to supercomputers, SoftwareX 1–2 (2015) 19–25.
[34] W. Humphrey, A. Dalke, K. Schulten, VMD: visual molecular dynamics, Mol. Graphics Modell. 14 (1) (1996) 33–38.
[35] C.Y. Legault, CYLview, 1.0 B, Université de Sherbrooke, 2009.
[36] P.J. Stephens, F.J. Devlin, C.F. Chabalowski, M.J. Frisch, Ab-Initio calculation of vibrational absorption and circular-dichroism spectra using density-functional force-fields, J. Phys. Chem. 98 (45) (1994) 11623–11627.
[37] S. Grimme, J. Antony, S. Ehrlich, H. Krieg, A consistent and accurate ab initio parametrization of density functional dispersion correction (DFT-D) for the 94 elements H-Pu, J. Chem. Phys. 132 (15) (2010) 154104.
[38] F. Weigend, R. Ahlrichs, Balanced basis sets of split valence, triple zeta valence and quadruple zeta valence quality for H to Rn: design and assessment of accuracy, Phys. Chem. Chem. Phys. 7 (18) (2005) 3297–3305.
[39] O. Yazyev, A.J. Austin, R. Cammi, C. Pomelli, J.W. Ochterski, R.L. Martin, Gaussian 09 (Revision E. 01), Gaussian Inc., Wallingford, CT, 2013, p. 3.
[40] T. Lu, F. Chen, Multiwfn: a multifunctional wavefunction analyzer, J. Comput. Chem. 33 (5) (2012) 580–592.
[41] R. Krishnan, J.S. Binkley, R. Seeger, J.A. Pople, Self-consistent molecular orbital methods. XX. A basis set for correlated wave functions, J. Chem. Phys. 72 (1) (1980) 650–654.
[42] A.D. McLean, G.S. Chandler, Contracted Gaussian basis sets for molecular calculations. I. Second row atoms, Z=11-18, J. Chem. Phys. 72 (10) (1980) 5639–5648.
[43] J.M. Wang, R.M. Wolf, J.W. Caldwell, P.A. Kollman, D.A. Case, Development and testing of a general amber force field, J. Comput. Chem. 25 (9) (2004) 1157–1174.
[44] J. Wang, W. Wang, P.A. Kollman, D.A. Case, Automatic atom type and bond type perception in molecular mechanical calculations, J. Mol. Graph. Model. 25 (2) (2006) 247–260.
[45] A.W.S. da Silva, W.F. Vranken, ACPYPE-AnteChamber PYthon Parser interfacE, BMC Res. Notes 5 (1) (2012) 367.
[46] L. Martinez, R. Andrade, E.G. Birgin, J.M. Martinez, PACKMOL: a package for building initial configurations for molecular dynamics simulations, J. Comput. Chem. 30 (13) (2009) 2157–2164.
[47] H.S. Park, Y.J. Kim, W.H. Hong, Y.S. Choi, H.K. Lee, Influence of morphology on the transport properties of perfluorosulfonate ionomers/polypyrrole composite membrane, Macromolecules 38 (6) (2005) 2289–2295.
[48] K. Dai, C. Ma, Y.M. Feng, L.J. Zhou, G.C. Kuang, Y. Zhang, Y.Q. Lai, X.W. Cui, W. F. Wei, A borate-rich, cross-linked gel polymer electrolyte with near-single ion conduction for lithium metal batteries, J. Mater. Chem. 7 (31) (2019) 18547–18557.
[49] H. Bouhamed, S. Boufi, A. Magnin, Alumina interaction with AMPS-MPEG random copolymers I. Adsorption and electrokinetic behavior, J. Colloid Interface Sci. 261 (2) (2003) 264–272.
[50] L.N. Wang, X.C. Zhan, Z.G. Zhang, K.L. Zhang, A soft chemistry synthesis routine for $LiFePO_4$–C using a novel carbon source, J. Alloys Compd. 456 (1–2) (2008) 461–465.
[51] W.W. Cui, D.Y. Tang, Electrospun poly(lithium 2-acrylamido-2-methylpropane-sulfonic acid) fiber-based polymer electrolytes for lithium-ion batteries, J. Appl. Polym. Sci. 126 (2) (2012) 510–518.
[52] L. Porcarelli, A.S. Shaplov, M. Salsamendi, J.R. Nair, Y.S. Vygodskii, D. Mecerreyes, C. Gerbaldi, Single-ion block copoly(ionic liquid)s as electrolytes for all-solid state lithium batteries, Appl. Mater. Interfaces 8 (16) (2016) 10350–10359.
[53] M. Meyer, C. Vechambre, L. Viau, A. Mehdi, O. Fontaine, E. Mourad, S. Monge, J. M. Chenal, L. Chazeau, A. Vioux, Single-ion conductor nanocomposite organic-inorganic hybrid membranes for lithium batteries, J. Mater. Chem. 2 (31) (2014) 12162–12165.
[54] J. Cao, Y.M. Shang, L. Wang, X.M. He, L.F. Deng, H. Chen, Composite electrospun membranes containing a monodispersed nano-sized TiO_2@Li^+ single ionic conductor for Li-ion batteries, RSC Adv. 5 (11) (2015) 8258–8262.
[55] S.Y. Li, P.H. Ma, X.L. Cui, Q.D. Ren, F.Q. Li, Studies on the thermal decomposition kinetics of $LiPF_6$ and $LiBC_4O_8$, J. Chem. Sci. 120 (2) (2008) 289–292.
[56] K. Zaghib, M. Dontigny, A. Guerfi, J. Trottier, J. Hamel-Paquet, V. Gariepy, K. Galoutov, P. Hovington, A. Mauger, H. Groult, C.M. Julien, An improved high-power battery with increased thermal operating range: C–$LiFePO_4$//C–$Li_4Ti_5O_{12}$, J. Power Sources 216 (2012) 192–200.
[57] T.T. Zuo, Y. Shi, X.W. Wu, P.F. Wang, S.H. Wang, Y.X. Yin, W.P. Wang, Q. Ma, X. X. Zeng, H. Ye, R. Wen, Y.G. Guo, Constructing a stable lithium metal-gel electrolyte interface for quasi-solid-state lithium batteries, Appl. Mater. Interfaces 10 (36) (2018) 30065–30070.